ROBUST CONTROL

(SC42015)

Control Design for a Floating Wind Turbine Part 1 - SISO Analysis and Control Design

---

Students

Daniel Varela - 5321263

Ibón Gracia Merino - 5358779

Responsible Instructor

J.W. van Wingerden

November 27, 2020

Contents

1 Introduction

The goal of this Assignment is to investigate the challenges and limitations in designing a control system for a floating wind turbine for normal operation [3].

For this first part, we consider a SISO system and design a controller that achieves reference tracking of a rotational velocity target by control of the angle of the blades of the Floating Wind Turbine while meeting all the design requirements.

During the design process, some of the fundamental limitations of SISO control arise, such as the influence of Right Half Plane zeros in the plant and the restrictions these impose, as well as the trade-offs necessary to design for different goals, such as reference tracking, disturbance rejection or noise attenuation. A few controllers have been designed and their performance will be compared through design tools such as Bode Plot and Root Locus, using the corresponding Matlab functions.

These limitations, as well as the controller design and results are discussed extensively in this document.

2 Plant Analysis and Limitations

2.1 Obtaining the SISO Plant

The first thing we must do before we start analysing the plant is to extract the SISO system from the given `.mat` file `Assignment_Data_SC42145.mat`. Importing the file to `Matlab` reveals the state-space model `FWT`, with three inputs (corresponding to blade pitch, β, motor torque, τ_e and wind disturbances, V, in this order), two outputs (rotational velocity, ω_r and position, z) and the corresponding matrices, `A`, `B`, `C`, `D`.

The SISO transfer function we're interested in analysing is the one that maps blade pitch to rotational velocity. These are, respectively first input and output of our state-space model. Knowing this, we can use the following commands to extract the corresponding transfer function from state-space matrices `A`, `B`, `C`, `D`:

```
>> [num,den] = ss2tf(A,B,C,D,1);
ans =

         0   -0.0799   -0.0033   -0.8677    0.0065   -0.0346
         0         0   -0.0487   -0.0348   -0.0750   -0.0520

>> Gp = tf(num(1,:),den)
```

```
Gp =

  -0.07988 s^4 - 0.003315 s^3 - 0.8677 s^2 + 0.006493 s - 0.03458
  ---------------------------------------------------------------
   s^5 + 0.5979 s^4 + 10.98 s^3 + 4.709 s^2 + 0.5421 s + 0.1827
```

As seen above, the transfer function of the plant we'll be working with during this report is:

$$G_P = \frac{-0.07988s^4 - 0.003315s^3 - 0.8677s^2 + 0.006493s - 0.03458}{s^5 + 0.5979s^4 + 10.98s^3 + 4.709s^2 + 0.5421s + 0.1827}$$

Before we proceed, we'd like to get a better grasp of the gain of our plant and the placement of the poles and zeros. Using the command `zpk(Gp)` allows us to do so. Finally, we obtain:

$$G_P = \frac{-0.079878(s^2 - 0.007693s + 0.04)(s^2 + 0.0492s + 10.82)}{(s + 0.4104)(s^2 + 0.02113s + 0.04101)(s^2 + 0.1664s + 10.85)}$$

2.2 SISO Plant Analysis

Having obtained the SISO Plant, we now look to analyse it. Notice that the gain is negative, meaning the controller will need negative gain to eventually stabilize our plant. For now, however, we assume no controller at all is added and proceed with the analysis. To do so, we plot the Root Locus and Bode Plots of the open loop uncontrolled system, using the `rlocus()` and `bode()` functions in `Matlab`. Both figures are presented below:

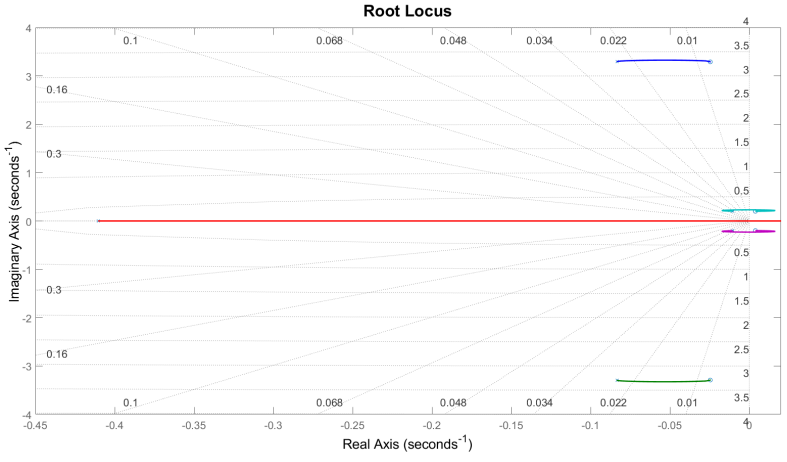

Figure 1: Root Locus of G_P

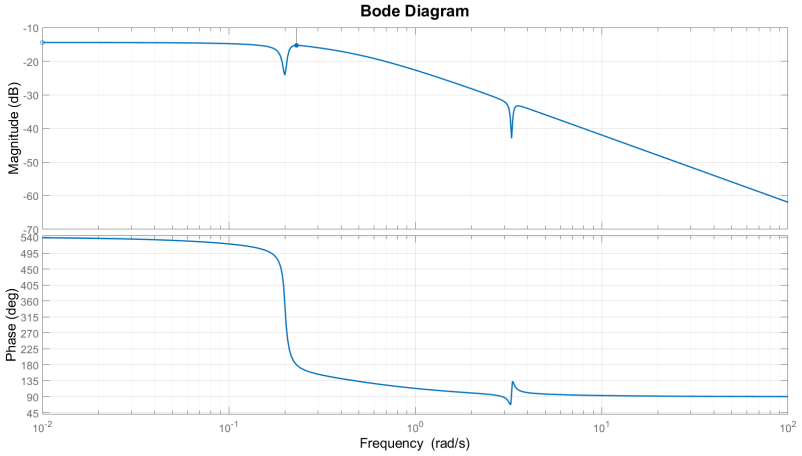

Figure 2: Bode Plot of G_P

We start by analysing the Root Locus (1). Immediately, we see a complex pair of zeros in the Right Half of the s-Plane. These zeros, along with the poles close to them, correspond to the platform tilt mode [1] of the wind turbine, and are detailed below. From sections 2.4 and 5.6 of [4] we find that these impose limitations on the performance of our system.

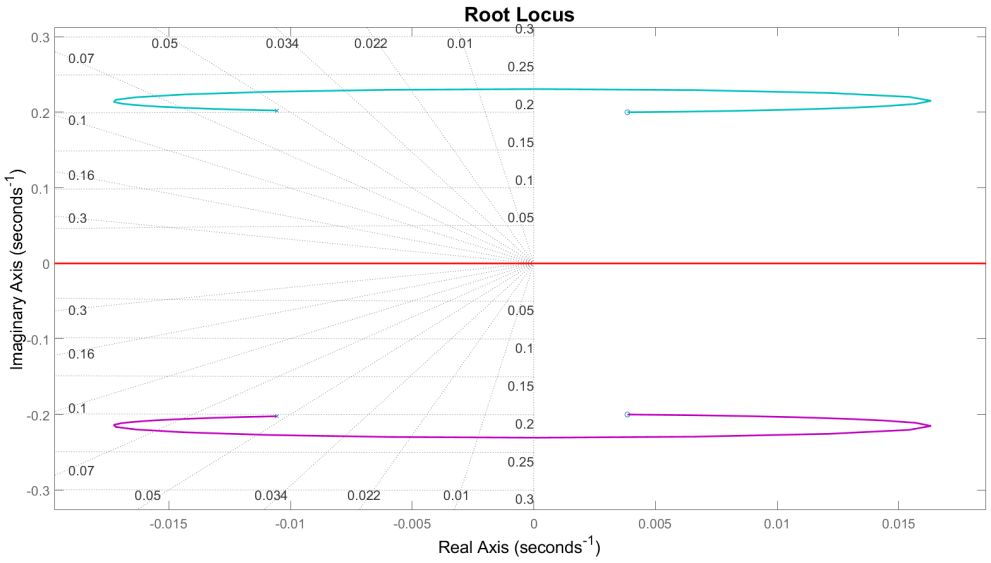

Figure 3: Detail of Right Half Plane Zeros in the Root Locus.

Specifically, since we have two RHP-zeros, the root locus tells us that, as the gain increases (for both negative and positive values of gain), the poles of the closed loop, which migrate from the poles to the zeros of the open loop plant will eventually cross the imaginary axis, destabilizing the system. Specifically, this gain, which corresponds to the crossing of the imaginary axis is also the gain for

which the crossover frequency ω_c of the plant L aligns with the steep drop in phase that happens in the Bode Plot (2). This drop in phase induces a crossing of the $180°$ line, further confirming that the plant becomes unstable in this region.

Further commenting on the zeros in the RHP, we know they are given by the term $(s^2 - 0.007693s + 0.04)$ in the transfer function G_P. This is a second order term, which places two poles at $s = 0.00385 \pm 0.2j$, meaning their frequency is $\omega = \|0.00385 + 0.2j\| \approx 0.2rad/s$. This is, again, confirmed by the bode plot, which drops $360°$ at around $\omega = 0.2rad/s$. Of these, $180°$ are the contribution of the right half plane zeros, and the other $180°$ are caused by the poles given by $(s^2 + 0.02113s + 0.04101)$, which have frequency $\omega = \| - .0106 \pm 0.202j\| \approx 0.2rad/s$ as well.

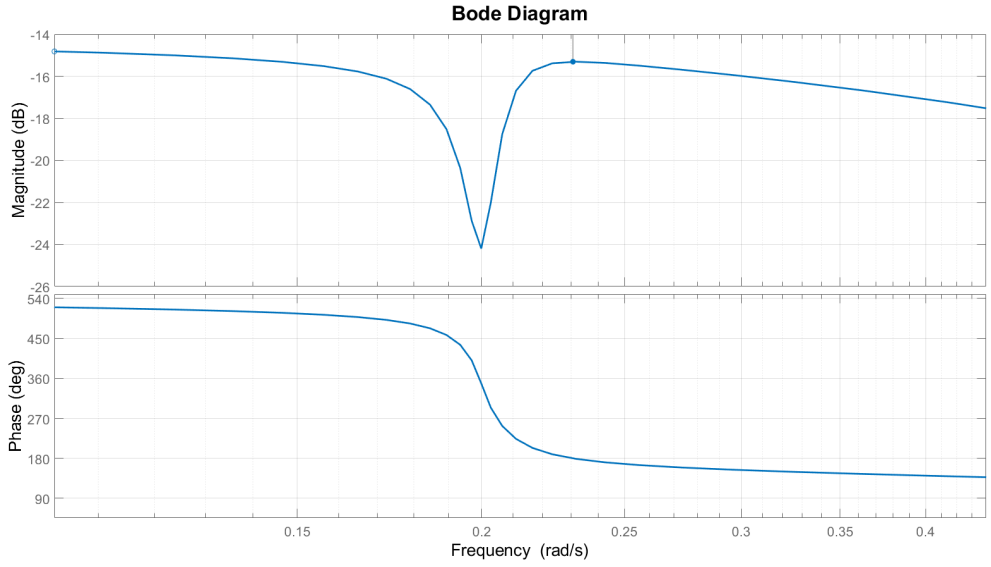

Figure 4: Phase Drop in the Bode Plot.

2.3 Bandwidth Limitations Imposed by Plant Design

So far, the analysis has revealed that the structure of zeros and poles of the plant imparts a steep drop in phase at $\omega \approx 0.2rad/s$. In practice, this means that trying to increase the crossover frequency, ω_c of our plant past $0.2rad/s$ would cause a crossing of the 180º line, destabilizing the system.

This design constraint isn't really easily liftable either. For instance, simply adding real zeros at the frequency $\omega = 0.2rad/s$ wouldn't do the trick because the slope these zeros impart in the phase margin isn't enough to counteract the phase drop. One could proceed by a process similar to plant inversion, placing 4 complex zeros, two on top of the poles at $s = -.0106 \pm 0.202j$, two mirroring

the RHP zeros, at $s = -0.00385 \pm 0.2j$. This controller isn't realizable (neither is the first one we discussed), and we'd need to add at least 4 extra zeros to make it so. Even then, having successfully countered the downwards slope in the phase, we'd have created a 4th order controller just for this, and we'd need to add further complexity on top of this already complex controller in order to stabilize and increase the cut-off frequency from here. This technique is also only possible if we know the exact transfer function of our system, which is often not the case, and it hides dynamics of the plant itself, which isn't always desirable.

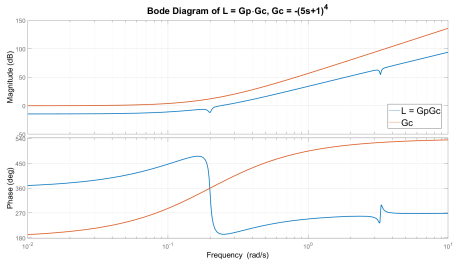

(a) Adding four zeros at $\omega = 0.2rad/s$ with $Gc = -(5s+1)^4$.

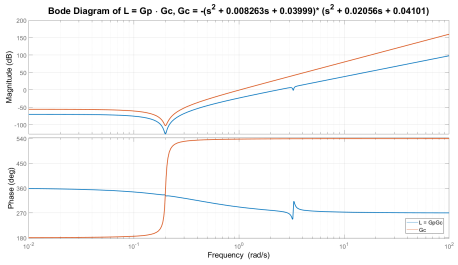

(b) Inverting the downwards slope of the phase plot with $Gc = -(s^2 + 0.007693s + 0.04)(s^2 + 0.02113s + 0.04101)$

Figure 5: Bode Plots of the Non-realizable controllers discussed, as illustration of the arguments made.

Instead of trying to go about it via plant inversion one could alternatively try to increase the gain so that it is as high as possible without getting past this barrier frequency $\omega = 0.2rad/s$. For a gain $K = -9.1$, we place the cut off-frequency at $\omega = 0.191rad/s$ and have a healthy $90°$ of phase margin, which, on paper, seems really good. Looking at the step response of this system, however, reveals a highly oscillatory response. A root locus plot for this system reveals the problem. The closed loop poles, for this gain value, are very close to the origin, provoking a highly oscillatory response despite the seemingly great phase margin and bandwidth values. Though we've only looked at a simple gain controller here, this limitation on performance of systems due to RHP-zeros is rather general, independent of controller, and is further expanded upon in section 4 of [6].

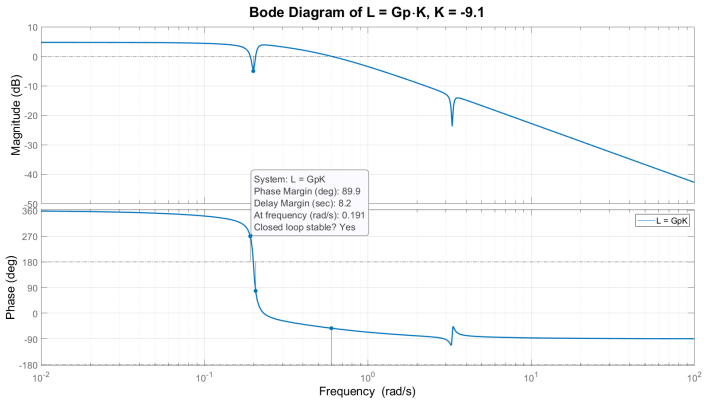

Figure 6: Bode Plot of $L = GpK$, $K = -9.1$

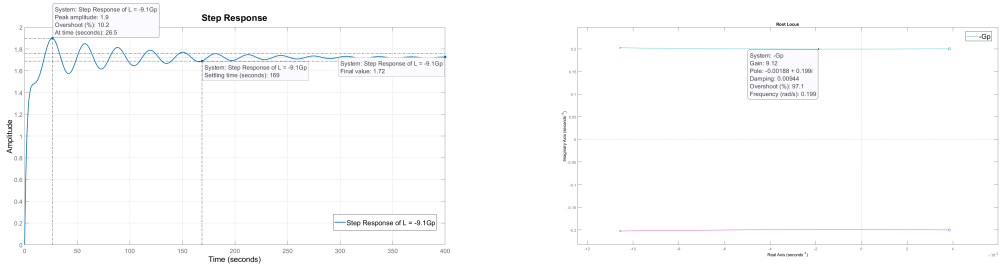

(a) Step Response

(b) Root Locus

Figure 7: Step Response and Root Locus Detail for gain $K = -9.1$.

We can, as further evidence, quantify the bandwidth limitations imposed by the RHP zeros. According to section 5.6.3 of [4], for a case like ours, where the imaginary part of the RHP zero is nearly 10 times higher than the real part, a conservative upper bound would be:

$$\omega_B \approx \omega_c < |z| = 0.2$$

All of this seems to indicate that achieving a bandwidth of $0.032Hz = 0.2rad/s$ or higher is a hard task due in particular to the two RHP-zeros in the plant's design. In the next section, we provide a physical explanation for this.

2.4 Physical Interpretation of Bandwidth Limitations

Previous sections have shown, from analysis of Bode and Root Locus plots, that the structure of the plant introduces a barrier to achieving bandwidth values higher than $f_B = 0.1Hz$, since there are 4 elements (two poles, two zeros) of the system positioned so that a very steep phase drop

happens around this area.

Section III.B of [1] allows us to get a better feel for how the plant works and a physical interpretation of this phenomena. The negative damping problem goes over how forwards sways of the turbine will result in faster relative wind speed. In turn, the blades will be pitched to prevent the generator speed from growing. This, however, reduces thrust, which causes the tower to sway further forwards. This generates a feedback loop that eventually destabilizes the system. In the linearized plant of the Wind Turbine, we see exactly this behaviour: as the gain grows in the blade angle controller, the tower plant becomes more unstable. [1] goes on to conclude that the control system bandwidth must be smaller than the frequency of the structure with the RHP-zeros to avoid instability. Smaller bandwidths can be achieved by detuning the pre-existing PI controllers in wind turbines, but this often comes at the expense of less power production [2].

This is an important conclusion, as it imposes restrictions on the design of our controller if we want to keep the structural integrity of the wind turbine, as poor generator speed tracking results in frequent shutdowns arising from the generator speed reaching its limit, as seen, again, in [1].

3 Converting Design Specifications to the Frequency Domain

The given specifications are reproduced below and will now be addressed one by one, in the same order in which they were tackled during the design process. We started by guaranteeing that the system could track references properly and without going over the overshoot requirements, and only after that focused on trying to reduce settling times.

- No steady state error.
- Overshoot $\leq 1\%$;
- Small Settling Time;

3.1 No Steady State Error

For this requirement, we again reference sections from [4]. Specifically, section 2.6.2 goes over design requirements in loop shaping for various types of reference signals. Here, we find that, to have no steady state error, we need as many integrators in our plant, $L(s)$, as integrators in the reference input.

Since the task is to track a reference step signal, $R(s) = \frac{1}{s}$, we need at least one integrator in our plant in order to achieve reference tracking. In terms of frequency requirements, this means that the slope of the magnitude curve $|L|$ need to be at least -1 for low frequencies ($\omega \to 0$) to correctly track step references (-2 for ramps, and so on). This is the requirement we'll be aiming for in the project.

3.2 Overshoot Smaller than 1%

To conclude about overshoot in the frequency domain, we briefly discuss the concepts of Total Variation and Excess Variation. In [4], these are defined as:

- Total Variation (TV): The total movement of the output.
- Excess Variation: The total variation (TV) divided by the overall change at steady state.

Looking at these two definitions, we can easily see their associations with the time response concepts of overshoot and decay or damping ratio. In this sense, higher values of TV correspond to higher overshoot values and less damped responses. A TV value of one represents a completely dampened response, with no overshoot. Since we want overshoot to be below 1%, we can translate this as a constraint on TV, where we want it to be as close to 1 as possible.
On the other hand, section 2.4.4 in [4] gives general bounds on TV values with respect to M_T, the maximum magnitude of the complementary sensitivity function:

$$T = \frac{G_P K}{1 + G_P K} \quad , \quad M_T = \max_{\omega} |T(j\omega)| = \|T\|_\infty$$

$$M_T \leq TV \leq (2n+1) M_T$$

It's clear to see that $TV \approx 1$ implies $M_T \leq 1$, since it works as a lower bound. This is a frequency constraint we can now use in our design. We know that the maximum of the magnitude curve of the closed loop transfer function needs to be around $0\ \mathbf{dB}$ if we hope to achieve an overshoot as small as indicated by the design specifications.

One can also, alternatively, discuss this result in terms the phase and gain margins of the open loop transfer function $L(s)$, using two relationships found in lecture 1, [5].

$$GM \geq 1 + \frac{1}{M_T} \quad , \quad PM \geq 2 \arcsin \frac{1}{2M_T}$$

Computing these with the upper bound $M_T \leq 1$, we easily obtain $PM \geq 60^\circ$ and $GM \geq 2 = 6.02\ \mathbf{dB}$.

A quick note: To achieve reference tracking in the previous section, the complementary sensitivity function must have $0\ \mathbf{dB}$ gain at low frequencies. This fact puts yet another constraint on the overall shape of T.

3.3 Small Settling Time

This constraint doesn't impose a hard number, and is much about trying to optimize the response after the two hard constraints have been met. The relationship between this constraint and the other two is important, however, and will be expanded upon in this subsection.

To get a smaller settling time we usually want a faster response. In general this can be translated by higher gain values. Increasing gain has the effect of shifting the magnitude of the bode plot up while not changing the phase plot. As so, increasing the gain also increases the crossover frequency of the system, and, in turn, also our system bandwidth, defined formally [4] as the point where the magnitude of the sensitivity function first crosses the $-3\ \mathbf{dB}$ line from below:

$$S = \frac{1}{1 + G_P K} \quad , \quad |S(j\omega_B)| = -3\ \mathbf{dB}$$

So far, it seems obvious that increasing the gain of our system improves settling times. However, this is where we start running into some problems. For most systems, increasing gain also usually leads to less phase margin, which makes the response more oscillatory. This can very easily conflict with the bound $PM \geq 60^\circ$ imposed by the overshoot requirement.

Further, the Bode integral formula (described, for instance, in section 14.2 of [7]) states that the area below and above the $0\ \mathbf{dB}$ line of the $|S(j\omega)|$ must be equal. Increasing bandwidth necessarily increases the area below the 0dB line of $|S(j\omega)|$, meaning the area above it will also increase (usually implying a higher peak M_S). Since, additionally, $|S(j\omega)|$ and $|T(j\omega)|$ can never differ by more than 1 because $S + T = I$ [5], a higher peak of M_S tends to result in higher values of M_T as well which, again, can easily conflict with the imposed restrictions from previous points. Finally, an increase in the peak of $|S(j\omega)|$ will amplify high frequencies, making the system more sensitive to noise, leading, again, to worse responses.

For these reasons, getting small settling times can be translated to the frequency domain as getting higher bandwidth for our system, and necessarily also a higher cut-off frequency, since $\omega_B \leq \omega_c$ [4]. However, this can have trade-offs, so the design requirement is to achieve a bandwidth as high as possible while still satisfying all other constraints.

4 Controller Design and Analysis

4.1 Uncontrolled Plant Analysis

For reference, for the analysis of the plant, this is the block diagram we considered.

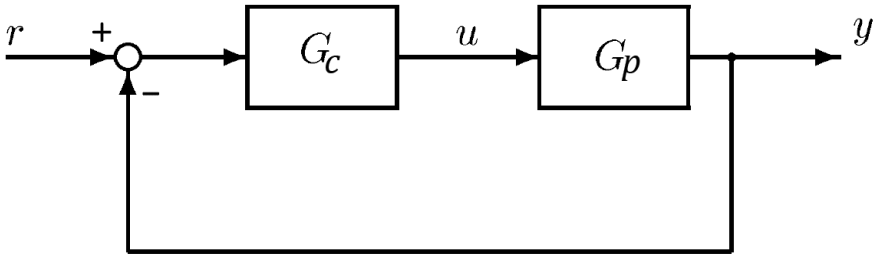

Figure 8: Step Response for the uncontrolled closed loop of $G_P(s)$

We start the analysis by looking at how the uncontrolled closed loop responds to a step input. Analysing those results, we notice that the response to a step yields a negative value, so we'll need to use a negative gain in our controller, as mentioned earlier in 2. Further, it's clear that the output isn't able to correctly track the input signal.

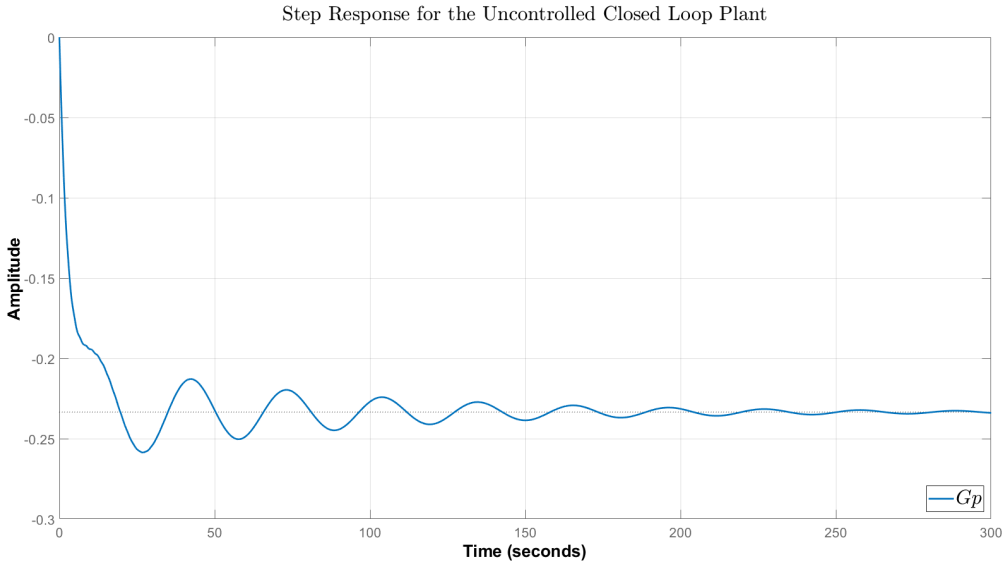

Figure 9: Step Response for the uncontrolled closed loop of $G_P(s)$

Having applied a negative gain $G_C = -1$ to the loop, we turn to the final theorem to see that, in order to achieve zero steady state tracking error, we'd need infinite gain values (in absolute value). Putting aside, for a moment, the clear impossibility of this task, we further see that a gain of

$G_C = -16.5$ destabilizes the plant, and therefore we cannot achieve higher gains than this.

$$e_{ss} = \lim_{s\to 0} sE(s) = s\frac{R(s)}{1 + G_P(s)G_C(s)} = \frac{1}{1 + G_P(s)G_C(s)} = \frac{1}{1 - 0.1893G_C(s)}$$

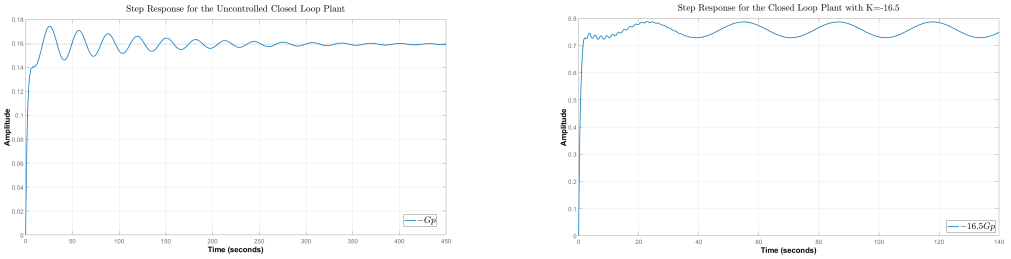

(a) $G_C = -1$.

(b) $G_C = -16.5$.

Figure 10: Step Responses of the closed loop plant for the gain values discussed.

4.2 Initial Design: Achieving Stability with an Integrator

As stated before, correct tracking of an error signal requires the slope of$|L|$ to be -1 at low frequencies, which we currently don't have. To correct for this, we start by adding an integrator to our design, in order to achieve the reference tracking specification. This is a controller with the structure:

$$G_{C1} = \frac{K_I}{s}$$

Applying this controller and adjusting the gain to $K_I = -.26$, we obtain the following results:

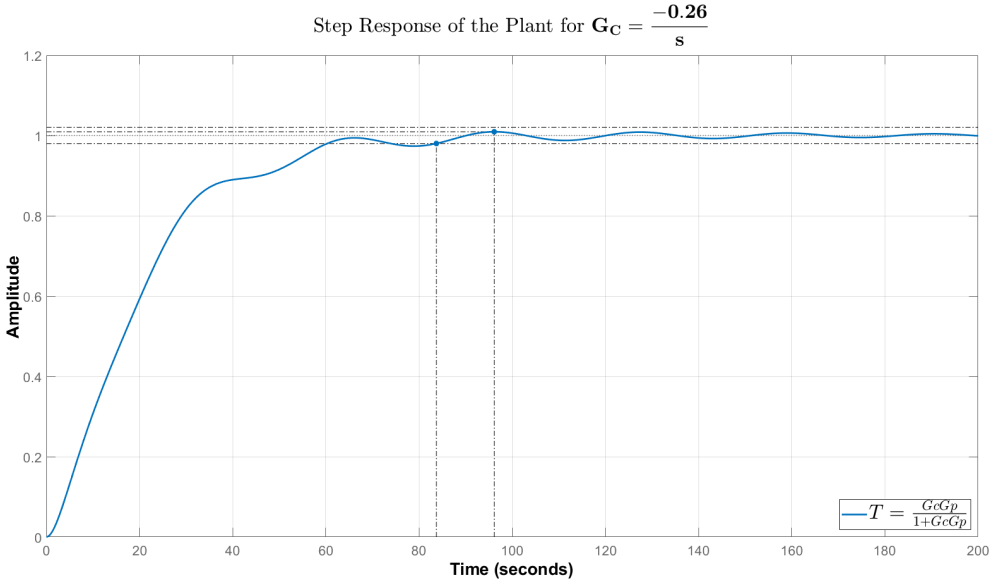

Figure 11: Step Response for $G_{C1} = \frac{-0.26}{s}$

Analysis of the results shows a clear improvement. With just a integrator, we're able to stabilize the plant, achieve reference tracking and less than 1% overshoot, while managing a settling time of $83.7s$. This is a slow response, in general, but the value makes sense, since the open loop root-locus shows that the dominant poles are very close to zero.

So far, the two hard specifications are met, and we get values that seem to be decent for settling time. To further inspect this design, we turn to the following bode plots:

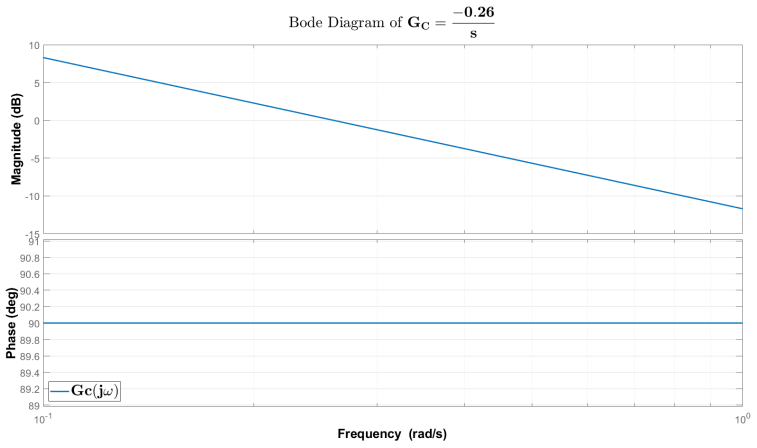

Figure 12: Bode Diagram of $G_{C1}(j\omega)$

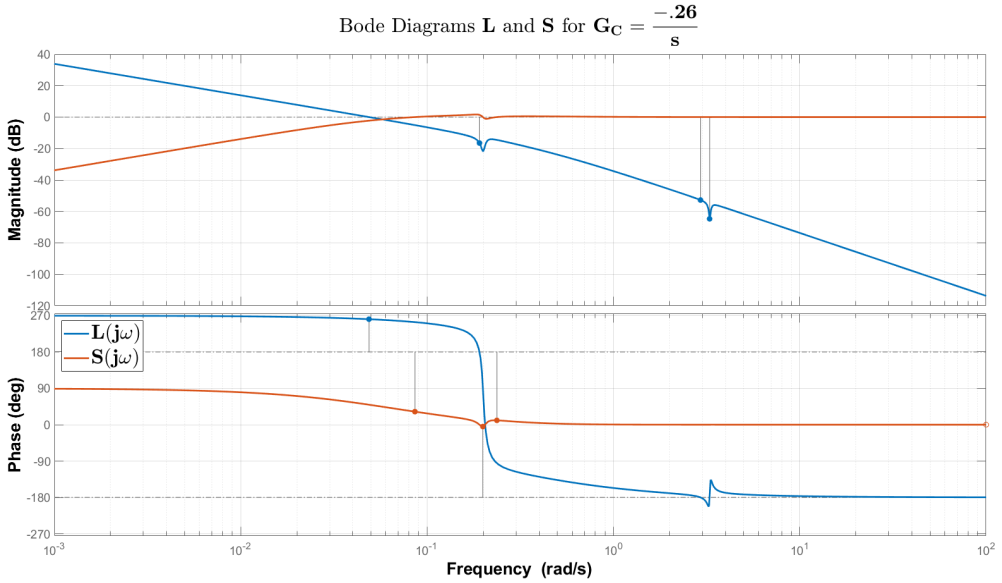

Figure 13: Bode Diagrams of $L(j\omega)$ and $S(j\omega)$

Looking at the Bode plot of the the open loop plant and the sensitivity function we have:

- Bandwidth, $\omega_B = 0.0428\ \mathbf{rad/s}$;

- Cut-off Frequency, $\omega_c = 0.0487\ \mathbf{rad/s}$;
- Phase Margin, $PM = 81.1°$
- Gain Margin, $GM = 16.5\ \mathbf{dB}$

Looking at $|L(j\omega)|$, we have a slope of $-20\ \mathbf{dB/decade}$ at low frequencies and near the crossover, and of $-40\ \mathbf{dB/decade}$ at frequencies higher than the cut-off frequency, which, again, is in line with the given specifications and within the general guidelines for Loop Shaping in [4].

4.3 Improving Settling Times using a 1st Order Filter

Looking at the step response of the previous controller, we see decent rise times, but the system oscillates more than desired close to the reference, which ultimately hinders settling times. Using this as motivation, the next step in the design was to add a filter to the system. Since, at high frequencies, the open loop curve $|L(j\omega)|$ is already dropping at around $-40\ \mathbf{dB/decade}$, adding a second order filter seems unnecessary. As so, we settled on a 1st order filter. As for the position of the new pole introduced, we can't have it too close to our current bandwidth ($\approx 0.04\ \mathbf{rad/s}$), because this would introduce unwanted phase-lag in this area, further reducing bandwidth and phase margins, which could actually have an effect opposite to what we're hoping to get. As so, we decide to place the pole to be around 10 times faster than the frequency of our current bandwidth. Tuning this position, we arrived at the final placement at $0.2\ \mathbf{rad/s}$. Doing so and tweaking the gain once again, we get the following results:

$$G_{C2} = \frac{K_I}{s(T_F s + 1)} = \frac{-0.225}{s(5s + 1)}$$

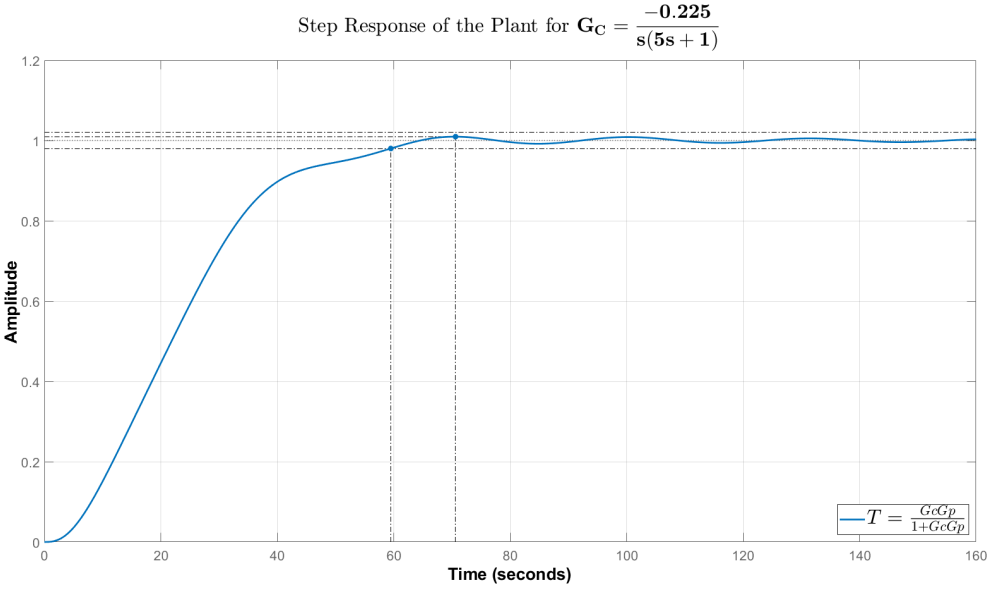

Figure 14: Step Response for $G_{C2}(s)$

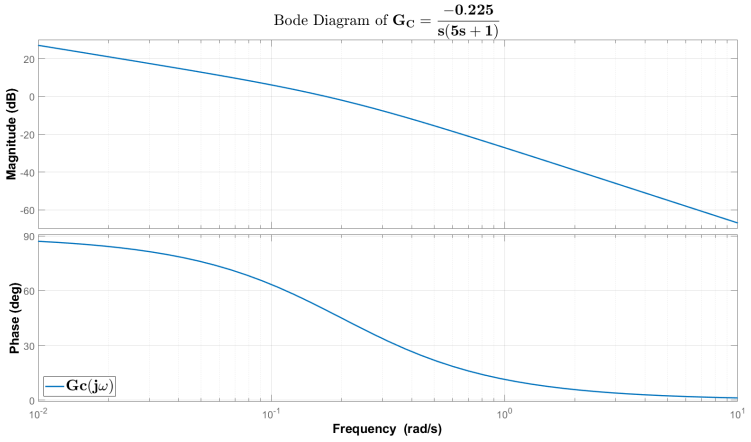

Figure 15: Bode Diagram of $G_{C2}(j\omega)$

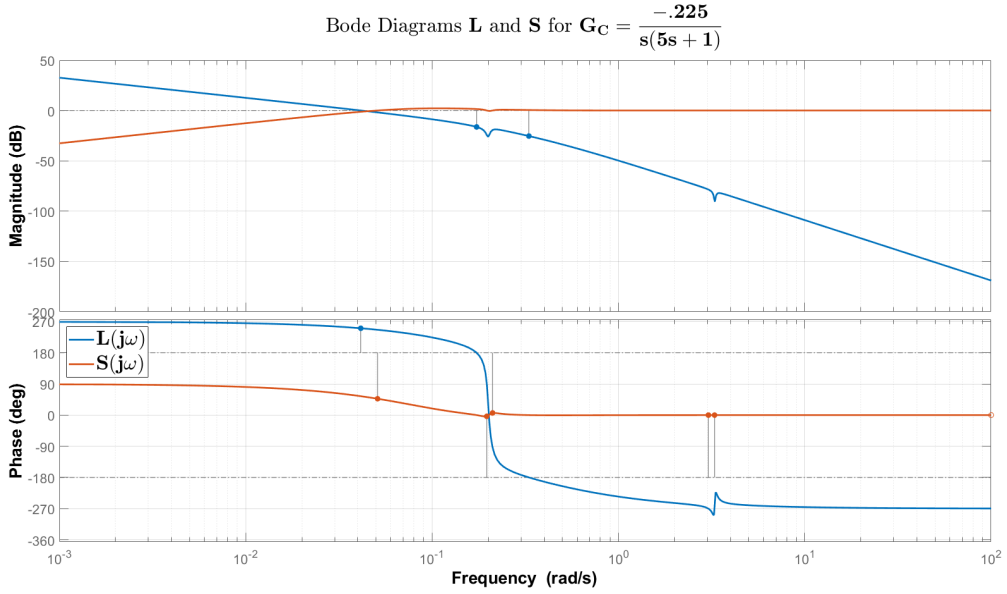

Figure 16: Bode Diagrams of $L(j\omega)$ and $S(j\omega)$

The main features of this design are summarized here:

- Overshoot, 0.945%;
- Settling Time, $59.5\ s$;
- Bandwidth, $\omega_B = 0.0325\ \mathbf{rad/s}$;
- Cut-off Frequency, $\omega_c = 0.0414\ \mathbf{rad/s}$;
- Phase Margin, $PM = 70.8°$;
- Gain Margin, $GM = 16.3\ \mathbf{dB}$;

By analysis of the step and frequency plots, we see that, in comparison to our previous controller, we still have a good shape for $|L|$. The slope is still -1 at low frequencies, it's now slightly steeper at the crossover and has slope -3 at high frequencies However, we do lose some phase margin and bandwidth. The rise time, as we'll see later in (4.5), is actually faster because the response oscillates less near the reference, however, it does take more time to start rising. Nevertheless, the filter seems to have done a decent job at reducing oscillations of the response, which results in a much improved settling time of $59.5s$.

4.4 Using Plant Inversion to Further Improve the Design

The previous controller, though achieving better results, seems to have lost some bandwidth and phase margin when compared to the values obtained by our simple integrator.
Inspired by the discussion had in section 2 about plant inversion, we remove the filter and introduce a notch control element with the objective of reducing the drop seen around $0.2\ \mathbf{rad/s}$. To do so, we cancel the slow poles in this region. These are given by the transfer function:

$$G_{P_1} = \frac{0.04101}{s^2 + 0.02113s + 0.04101} = \frac{\omega^2}{s^2 + 2\beta_1\omega s + \omega^2}, \quad , \quad \begin{cases} \omega = 0.02025\ rad/s \\ \beta_1 = 0.0521 \end{cases}$$

Using this information, we'll use the parameters ω and β_1 for the numerator of the notch controller, tweaking the parameter β_2 from the integrator and the gain K_I. The full controller structure is as follows:

$$G_C = \frac{K_I}{s} \cdot \frac{s^2 + 2\beta_1\omega s + \omega^2}{s^2 + 2\beta_2\omega s + \omega^2}$$

After tuning parameters to $\beta_2 = 0.295$ and $K_I = -0.3128$, we obtain the following results:

$$G_{C3} = \frac{-0.3128(s^2 + 0.02109s + 0.04101)}{s(s^2 + 0.1195s + 0.04101)}$$

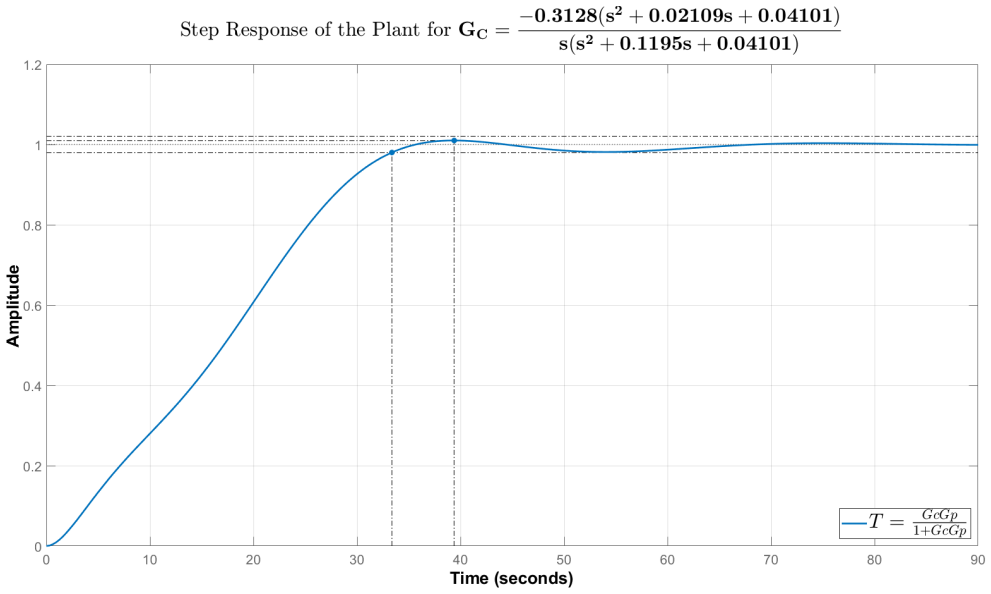

Figure 17: Step Response for $G_{C3}(s)$

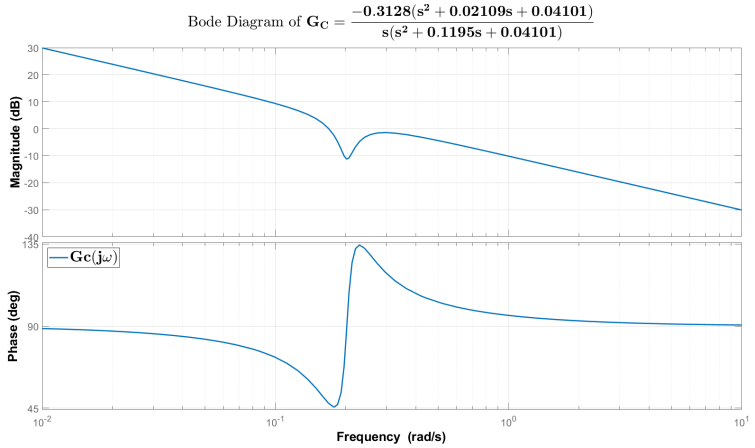

Figure 18: Bode Diagram of $G_{C3}(j\omega)$

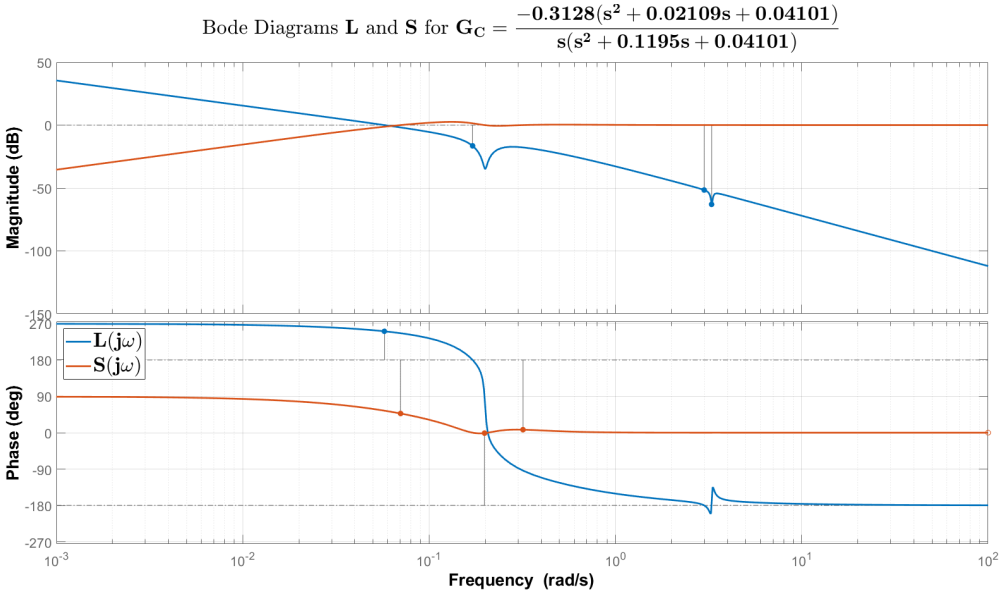

Figure 19: Bode Diagrams of $L(j\omega)$ and $S(j\omega)$

The main features of this design are summarized here:

- Overshoot, 0.911%;
- Settling Time, $33.4\ s$;
- Bandwidth, $\omega_B = 0.0454\ \mathbf{rad/s}$;
- Cut-off Frequency, $\omega_c = 0.0576\ \mathbf{rad/s}$;
- Phase Margin, $PM = 76.6°$;
- Gain Margin, $GM = 16.5\ \mathbf{dB}$;

Cancelling the slow poles in the left half plane yields very satisfactory results. Looking at the time response, we've eliminated the slow rising start of $G_{C2}(s)$, and as a result, achieve better settling times than either of the two previous controllers. The system response is also far less oscillatory than previous controller attempts.

Bode plots reveal a similar picture. Both bandwidth and cross-over frequencies are improved, as is the gain margin and the phase margin, relative to the $G_{C2}(s)$. Looking at the $|L|$ curve, we meet all necessary loop shaping specifications: slope of -1 for low frequencies and around crossover region, with a steeper slope of -2 at higher frequencies.

4.5 Comparing Results

Below are plots of step response, open loop transfer-function and sensitivity function for all three controller designs described above, to allow for a better comparison of the results obtained. Other designs were attempted, but were either worse than what's been presented, or far more complex than necessary for the diminishing returns they produced.

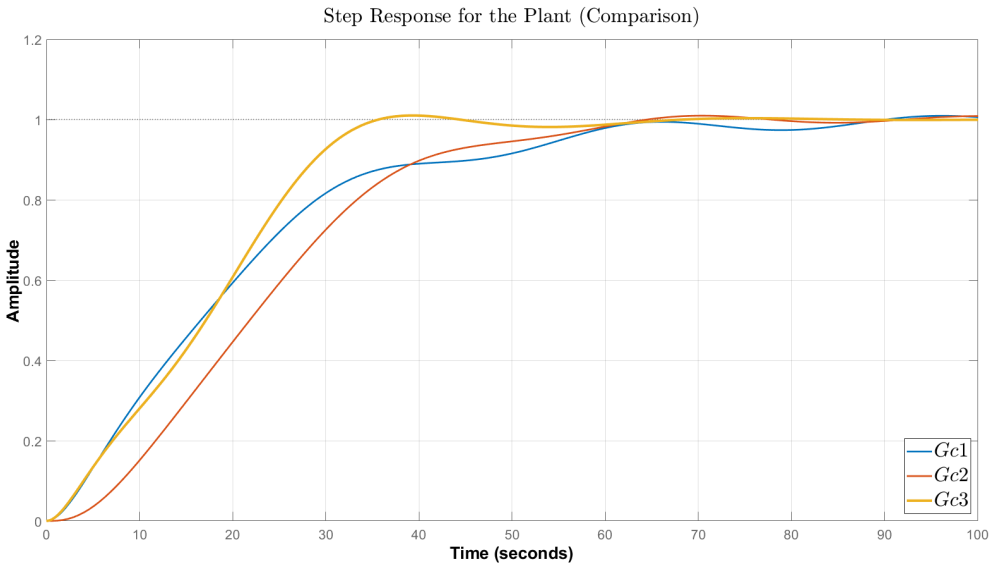

Figure 20: Step Responses for the various controllers

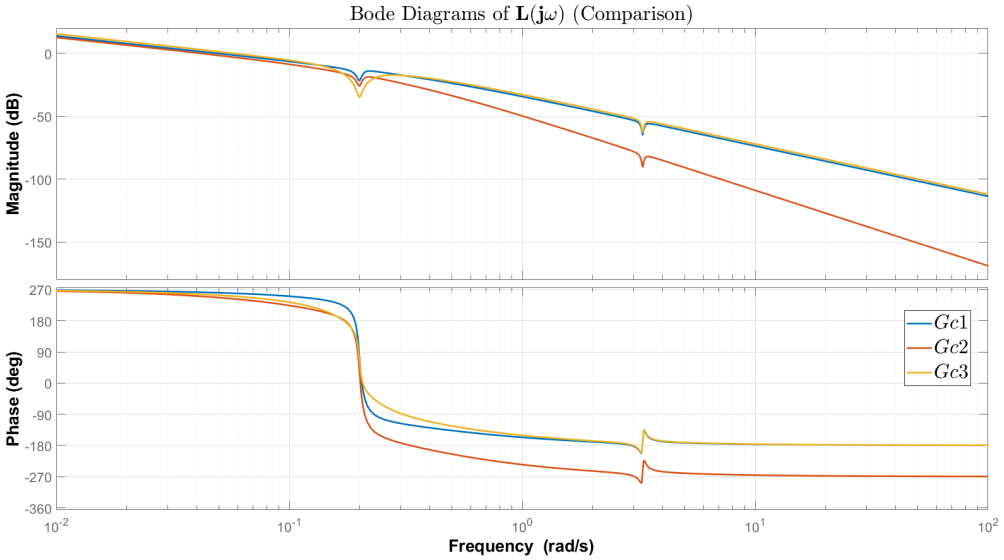

Figure 21: Bode Diagrams of $L(j\omega)$

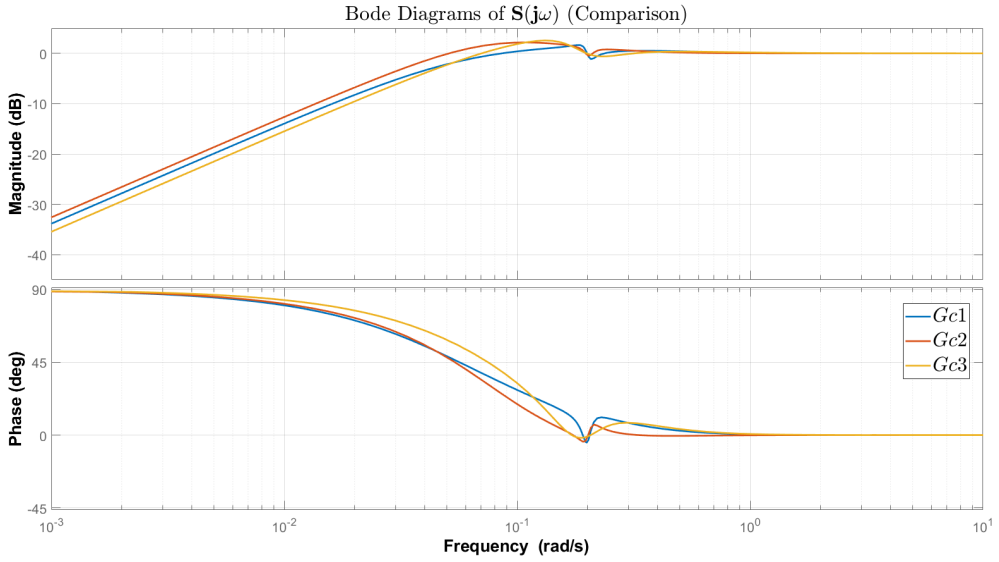

Figure 22: Bode Diagrams of $S(j\omega)$

Results achieved in the time and frequency domain can be seen below. As extra information, we also show values for ω_{BT} and M_T, even though no plots are shown of the Complementary Sensitivity curve. This is because the restrictions on $|T(j\omega)|$ could equivalently be seen in $|L(j\omega)|$ or $|S(j\omega)|$. Further, M_T and ω_{BT} aren't usually as good as M_S, ω_B or ω_C when it comes to performance analysis [4].

G_C	Overshoot (%)	Settling Time (s)	Rise Time (s)
1	0.919	83.7	42
2	0.945	59.5	32.2
3	0.911	33.4	24.8

Table 1: Time Domain Properties

G_C	$\omega_B(\mathbf{rads/s})$	$\omega_c(\mathbf{rads/s})$	$\omega_{BT}(\mathbf{rads/s})$	$PM(^\circ)$	$GM(\mathbf{dB})$	$M_S(\mathbf{dB})$	$M_T(\mathbf{dB})$
1	0.0428	0.0487	0.0582	81.1	16.5	1.64	0
2	0.0325	0.0414	0.0640	70.8	16.3	2.16	0
3	0.0454	0.0576	0.0904	76.9	16.5	2.55	0

Table 2: Frequency Domain Properties

As a final note on this, we comment a bit on the improvements seen between controllers G_{C1} and G_{C3}. Both show quite similar frequency domain behaviour, so the vast improvements might not be clear. Looking a detail of Root Locus plot of both helps clarify things.

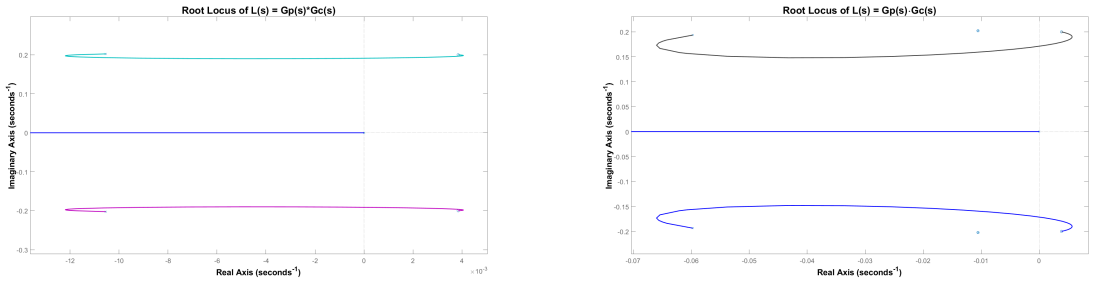

(a) $L(s) = G_P(s)G_{C1}(s)$ (b) $L(s) = G_P(s)G_{C3}(s)$

Figure 23: Root Locus Details for the poles and zeros closest to the imaginary axis.

Here, it's clear to see that the pole cancellation technique allows for the roots of the Root Locus plot to be "pulled" further into the Left Half Plane. This, in turn, allows us to increase the gain further and keep dominant poles of the closed loop farther away from the imaginary axis, thus achieving a faster, less oscillatory response.

5 Disturbance Rejection Problem

5.1 Introduction

In this section, the capabilities of the controller to reject disturbances will be studied. Rejecting disturbances means that the output error of the system will asymptotically go to zero when a disturbance is applied to the plant. Also the quality of the response will determine if the disturbance rejection capabilities of the plant are adequate, in the general time domain indicators, as settling time, damping, etc.

5.2 Disturbance Rejection Performance of the Developed Controllers

The disturbance transfer function was extracted from the `FWT` state space model employing the same procedure described in section 2, but this time we were interested in the transfer function that maps input signal 3 (Wind, V) to output 1 (Rotational Velocity ω_r). The transfer function, in this situation, is as follows:

$$G_V = \frac{0.2204(s^2 + 0.00128s + 0.04)(s^2 + 0.1053s + 10.82)}{(s + 0.4103)(s^2 + 0.02109s + 0.04101)(s^2 + 0.1665s + 10.86)}$$

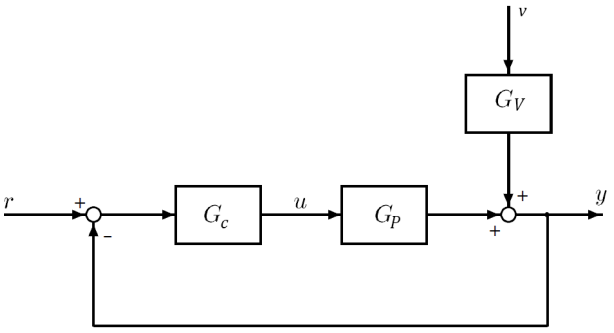

Figure 24: Diagram Considered for the Disturbance Rejection Problem.

Since an input in the wind velocity channel will result in an output rotational velocity change, we adapt the system plant (8) to accommodate the output from G_V as an output disturbance in the control loop we've been studying so far. The transfer function that maps this output disturbance to the output y can easily be obtained and is as follows:

$$\frac{y}{v} = G = G_V S = \frac{G_V}{1 + G_P G_C}$$

To evaluate the disturbance rejection properties of the controller structures presented previously, we apply a step input (representing a wind disturbance step) to the transfer function above, using all three controllers, and plot the respective results.

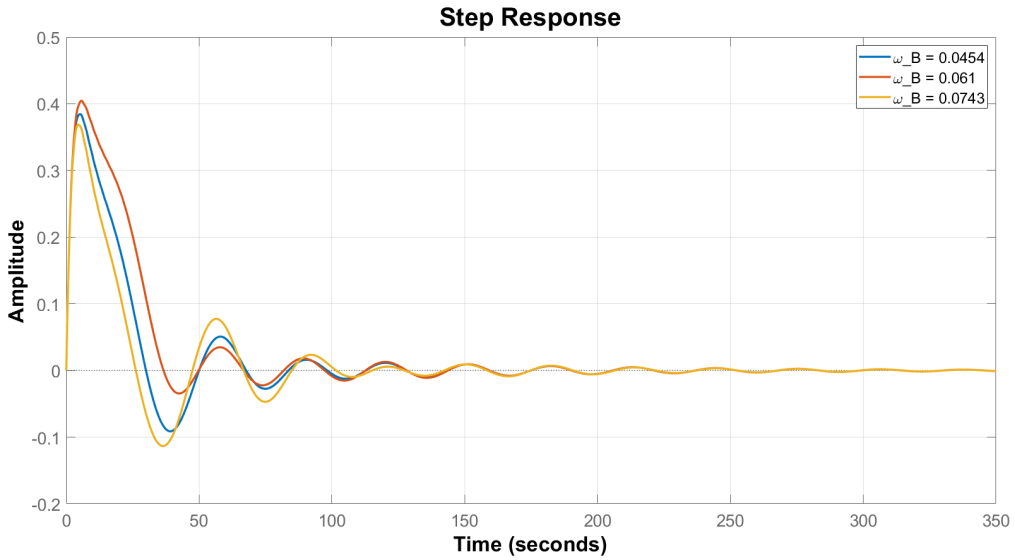

Figure 25: Step disturbance response for different bandwidths

G_C	Peak Response (%)	Under 10% (s)	Under 2% (s)
1	0.406	33.3	168
2	0.442	35.9	153
3	0.405	30.4	154

Table 3: Time Domain Properties

Looking at the responses and the values in the table above, we see that the controllers are able to reject step disturbance. However, their performance is not ideal, as evidenced by the relatively large amplitude and settling time and low damping of oscillations.

5.3 General Considerations on the Loop Shaping Problem

In order to conclude about changes to our controller for the disturbance rejection case, we first present the general framework of disturbance the rejection problem. The following figure shows the block diagram of a closed loop system with an input reference, output disturbance and measurement noise:

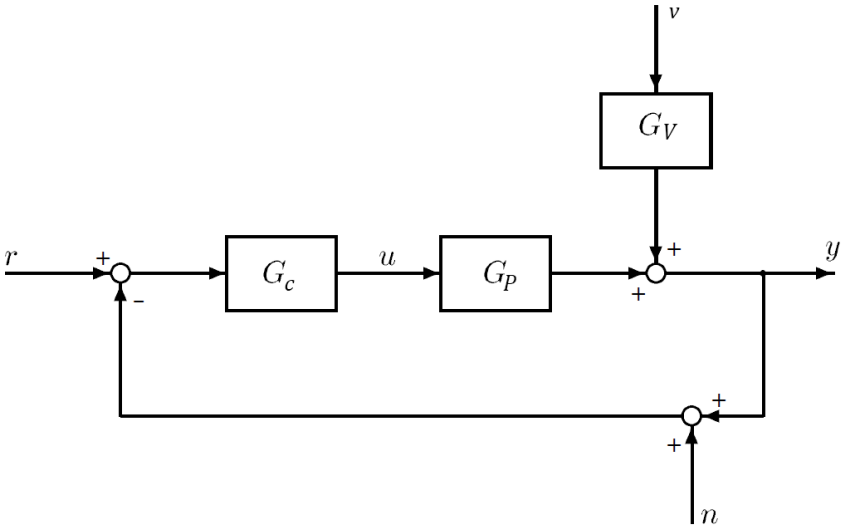

Figure 26: Block diagram of the general framework of the tracking and disturbance rejection problem [3]

The transfer function of the output error is therefore related to the reference input, disturbance and measurement noise through to following relation in the frequency domain:

$$e = -\frac{1}{1+L}r + \frac{G_V}{1+L}v - \frac{L}{1+L}n = -Sr + G_V Sv - Tn \tag{1}$$

In this equation, it can be observed that reference tracking and disturbance rejection require $S \approx 0$, which means L has to be large. However, this also implies that that T will be large, and therefore measurement noise is amplified. These two objectives of, on one hand, disturbance rejection and reference tracking and, on the other hand, noise attenuation, are contrary and therefore the solution achieved through the loop shaping procedure needs to be a trade-off between both objectives. Another objective in conflict with disturbance rejection and reference tracking is the minimization of control inputs, which grows with the control gain and, therefore, with L. In the following table the different requirements for the loop transfer function and the controller gain are shown [3]:

Design objective	Requirement on loop shape
Disturbance rejection	$\|L\|$ large
Reference tracking	$\|L\|$ large
Stabilization of an unstable plant	$\|L\|$ large
Measurement noise mitigation	$\|L\|$ small
Small input signals	Small $\|K\|$ and $\|L\|$
Physical controllers must be strictly proper	$\lim_{\omega\to\infty} \|L\| = 0$
Existence of RHP zeros or time delays	$\|L\|$ small (bandwidth limitation)
Existence of uncertain or unmodelled dynamics	$\|L\|$ small

Table 4: General requirements on the loop shape

As it has been indicated, some of these objectives are contrary. However, since different objectives tend to restrict different frequency regions, a good trade-off solution, which mostly satisfies all objectives can be found if the shape of L is designed in a different way in every frequency range. In general, high gains at low frequencies will provide good reference tracking and disturbance rejection whereas low gains at high frequencies will lead to good attenuation of (high frequency) measurement noise. The particular frequency range that separates the high frequencies from the low ones is the crossover range, which is defined as the region between ω_c (frequency at which the gain crosses 0 dB line) and ω_{180} (frequency at which the phase crosses -180º). In addition to this, as evidenced in section 2, the maximum bandwidth achievable is limited by the existence of RHP zeros. After the crossover region it is desirable that the magnitude of L has a steep negative slope, called high-frequency roll off [4]. In general, when it comes to bandwidth and gain of the open loop transfer function it can also be said that:

	Reference tracking	Disturbance rejection
High bandwidth	Successful tracking of higher frequency references	Disturbances attenuated in a wider range
High gain	Faster response to changes in reference and larger overshoot	Faster attenuation of disturbances

Table 5: Influence of bandwidth and gain of the loop transfer function

Care needs to be taken also when designing the loop shape in the crossover region. In [3] it is proved that the steeper the gain slope in the crossover region, the lower the phase margin, and so

more oscillating the response will be. This effect is worse if the slope before and after the crossover region is higher and in the presence of RHP zeros or delays, that deteriorate phase margin. A good value for the slope of the gain curve in the bode plot around the crossover region is -1. Also, in [7] it's stated that the area under the curve of the magnitude of the sensitivity function must be equal to the area over it. This means that an attempt to increase the bandwidth will lead to a higher peak in the crossover region, leading to oscillatory behaviour and ultimately to instability.

At low frequencies, the shape, and more specifically, the slope of the magnitude of the loop transfer function will depend on the type of signals (references, disturbances) the controlled system needs to be designed for. If these signals are steps, the open loop system must be at least type 1, this is, have one integrator. In this case, the slope of the gain curve at low frequencies will be -1. If the reference or disturbance is a ramp, the open loop system needs to be type 2 at least, having the gain curve a slope of -2 at low frequencies, and so on. This is usually done adding integrators in the controller transfer function. The controller that has been designed for this assignment has one integrator, so the loop transfer function is type one, and therefore the system will be able to follow steps in both reference and disturbances.

The two zeros also contribute to the slope of the gain curve, making it more positive. If we are to design a controller in such a way that the slope of $|L|$ is kept at -1, this means we have to introduce lag elements to counter the effect of the RHP zeros in the gain curve. However, these elements also decrease phase margin and, therefore, RHP zeros need to be taken into account when designing the shape of this region.

5.4 Controller Design for Disturbance Rejection

There exists a loop shaping method specifically oriented towards disturbance rejection. This procedure [3] takes into account (1) in the in which both reference and noise inputs are null and we have worst-case disturbances. It can be proved that in order to obtain an output error lower than some bound, the following relation must hold:

$$|L + 1| \geq |G_V| \tag{2}$$

values of L should lead to smaller output errors. However, in order to limit measurement noise amplification and controller input signals, it is preferable not to increase gain too much. The equation above fixes, therefore, a lower bound on the Loop transfer function that can be taken as a

starting point in the loop shaping process. From there, higher gain can be added to the low and mid-frequency regions and integrators in order to set the slope of the loop gain at low frequencies and, therefore, reject a specific type of disturbance. If the value of $|G_V|$ is larger than one, the last equation can be approximated as $|L| \geq |G_V|$, and it's easier to shape the controller transfer function making use of plant inversion, nevertheless, our disturbance transfer function shows a gain curve below 0 dB for all ω, so the method in this case is not that straightforward. Considering our plant and controller, this condition can be checked using the Bode plot of both $1 + L$ and G_V and looking at the magnitude plot:

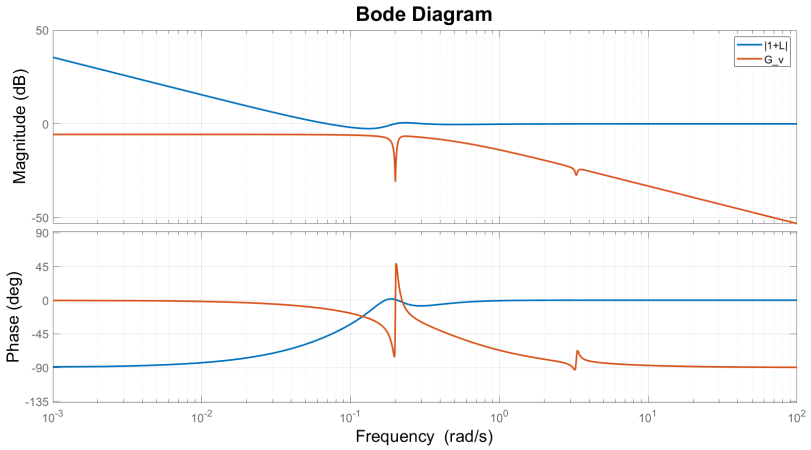

Figure 27: Bode plot of the disturbance transfer function and 1+L.

As it can be observed, the inequality is satisfied with a large margin, so our controller would be considered as a starting point to tackle the disturbance rejection problem. This feature of the disturbance-to-output transfer function will also lead to small disturbance amplification.

According to what has been explained before, the requirements on the shape of the loop transfer function for disturbance rejection are similar to the ones for a reference tracking controller. What makes a difference between both designs can be mainly observed in table 5. According to that table, when the controller is designed for disturbance rejection, the design will be an attempt to obtain a bandwidth as large as possible (in this assignment limited by the features of the plant) with high low frequency gain, whereas in the case of reference tracking, the design bandwidth is limited by the appearance of greater overshoot as the gain is increased, which goes against the specifications, so the bandwidth has to be small enough to not lead to undesirably large overshoot if the slope of the gain in the crossover region is kept. Therefore, when designing for disturbance rejection, where overshoot isn't as much of an issue, the bandwidth is designed to be higher than in the tracking

problem, so trying to achieve better reference tracking means losing tracking performance (mainly larger overshoot). Furthermore, when increasing the bandwidth of the open loop transfer function, oscillations will arise, and so care needs to be taken regarding phase margin. This is illustrated in the following Bode plot:

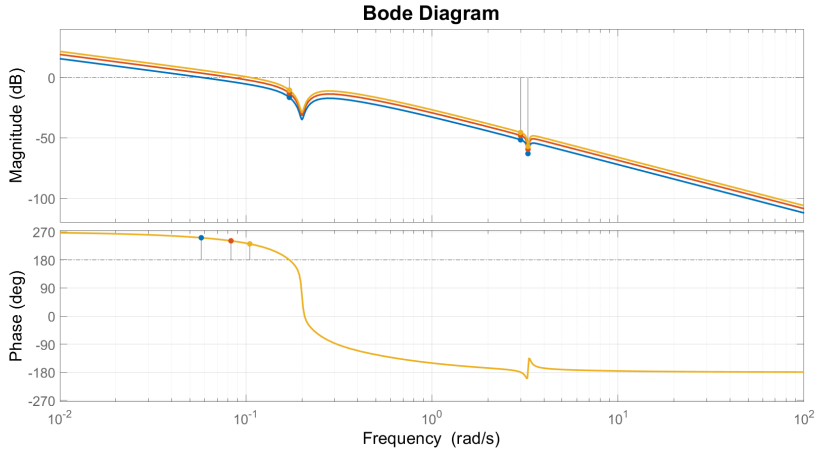

Figure 28: Bode plot of the loop transfer function. An increase in the bandwidth leads to less phase margin.

For example, adding a lead compensator would reduce oscillations and allow higher bandwidths to be achieved. If the bandwidth is increased, the attenuation of the disturbance is faster, leading to a lower peak, but the oscillation problem gets worse. This behaviour is related to the loss of phase margin and will be explained in the next sections.

5.5 Conclusions on the Use of the Designed Controllers for Disturbance Rejection

To conclude this section, it has been discussed that the disturbance rejection performance could be enhanced by increasing the bandwidth and gain, at the expense of reducing tracking capabilities. If the objective was only to reject step disturbances, the controller could be modified as stated in the previous section in order to obtain a “better controller” from the point of view of disturbance rejection. Nevertheless, if the controller should also meet the requirements stated in question 1 for reference tracking, the controller designed in this assignment would suffice, as all the requirements are accomplished and also the controller is able to reject step disturbances (with, however, relatively large amplitude and settling time). If the tracking requirements were relaxed, mainly in overshoot, an intermediate controller could be found that also rejects step disturbances with lower amplitude and settling times.

References

[1] I.A. Couchman G.J. van der Veen and R.O. Bowyer. Control of floating wind turbines. *American Control Conference, Montreal, Canada*, 2012.

[2] J.M. Jonkman. Influence of control on the pitch damping of a floating wind turbine, 2012.

[3] Robust Control [SC42145]. Practical assignment: Control design for a floating wind turbine, 2020.

[4] S. Skogestad and I. Postlethwaite. *Multivariable Feedback Control: Analysis and Design*. John Wiley and Sons, Chichester, England, 2 edition, 2005.

[5] J.W. van Wingerden. Lecture slides on robust and multivariable control [sc4015], 2020.

[6] K. J. Åström. Limitations on control system performance. *European Journal of Control*, 6(1), 2000.

[7] K. J. Åström and R. M. Murray. *Feedback Systems - An Introduction for Scientists and Engineers*. Princeton University Press, 2 edition, 2005.